$^{88}Sr^{+}$ single-ion optical clock with a stability approaching the quantum projection noise limit

Pierre Dubé,[1,*] Alan A. Madej,[1,2] Andrew Shiner,[1,2] and Bin Jian[1,2]
[1]*National Research Council Canada, Ottawa, Ontario, Canada K1A 0R6*
[2]*Department of Physics and Astronomy, York University, Toronto, Ontario, Canada M3J 1P3*
(Received 19 June 2015; published 22 October 2015)

A number of optical frequency standards have been evaluated with fractional uncertainties between 10^{-17} and 10^{-18}. Reduction of the statistical uncertainty of a clock comparison to this level is challenging, requiring the best possible stability to avoid excessively long averaging times. We report recent improvements of our $^{88}Sr^{+}$ single-ion standard that have reduced its 1-s Allan deviation from 1×10^{-14} to 3×10^{-15}, yielding an order of magnitude decrease in averaging time for a given statistical uncertainty level. Among the improvements made are the implementation of a clear-out laser that transfers the ion from the metastable state to the ground state at each cycle, followed by a state preparation step that transfers the ion to the ground-state magnetic sublevel of the probed transition. With these changes, the ion clock transition interacts with the probe laser at every interrogation cycle. The stability of our optical standard is essentially limited by the quantum projection noise for pulse lengths up to ≈ 100 ms.

DOI: 10.1103/PhysRevA.92.042119 PACS number(s): 06.20.−f, 06.30.Ft, 42.50.Lc, 37.10.Ty

I. INTRODUCTION

The development of optical atomic frequency standards has been phenomenal during the past decade, with evaluated uncertainties now reaching the 10^{-17} to the 10^{-18} level in fractional frequency units [1–11]. As a consequence, the demands on clock stability have also increased dramatically.

Single-clock stabilities of 2 to $3 \times 10^{-16}/\sqrt{\tau}$ have been demonstrated with optical lattice clocks, when a thousand or so trapped atoms are interrogated with an ultrastable laser with a long coherence time [6,11]. Although single-ion optical clocks have uncertainty levels comparable to those of lattice clocks [1,2,4,5,7], the single-particle optical references offer a significantly smaller signal-to-noise ratio to steer the local oscillator frequency. Stabilities of 2 to $3 \times 10^{-15}/\sqrt{\tau}$ have been achieved with single-ion clocks [1,2].

The optical clock studied at the National Research Council of Canada is based on the $5s\,^2S_{1/2}$-$4d\,^2D_{5/2}$ electric-quadrupole-allowed transition of a single $^{88}Sr^{+}$ ion. Recent work in the control and evaluation of the uncertainties of the S-D transition have reduced the fractional frequency uncertainty to 1.2×10^{-17} [4,7,12]. It is expected that the total uncertainty of the $^{88}Sr^{+}$ clock transition can be reduced to $\lesssim 3 \times 10^{-18}$ with an improved evaluation of the blackbody radiation (BBR) field [7]. Optimization of the frequency stability becomes crucial for the comparison of two similar clocks with such a low uncertainty level.

In this paper we present results of the recent improvements made to the stability of our $^{88}Sr^{+}$ single-ion optical frequency standard, with an observed performance that approaches the quantum projection noise (QPN) limit for 100-ms pulses. Details of the pulse sequence, state preparation step, interrogation method, and stability measurements are presented. A density matrix model of the atomic response is used to compare the observed stability to theory for our experimental conditions.

*pierre.dube@nrc-cnrc.gc.ca

II. EXPERIMENTAL METHODS

A. The $^{88}Sr^{+}$ optical frequency standard

Figure 1 shows the energy-level diagram of the $^{88}Sr^{+}$ ion, with the transitions and laser wavelengths used in the experiments presented here. The reference transition in the $^{88}Sr^{+}$ ion has a natural linewidth of 0.4 Hz caused by the $^2D_{5/2}$ metastable state lifetime of $\tau_{\rm ion} = 0.3908(16)$ s [13]. A small magnetic field of 1 to 2 μT is applied to the ion to split the clock transition spectrum into ten Zeeman components. The Zeeman spectrum is probed using an ultrastable laser source at 674 nm [14]. Usually, three symmetric pairs of Zeeman components are probed to cancel the first-order Zeeman shift, the electric-quadrupole shift, and other tensor shifts [12,15]. The laser can resolve Fourier-transform-limited spectra of 4 Hz on single Zeeman components for measurement times of ∼100 s [12,14].

The ion is cooled using a frequency-stabilized diode laser at 422 nm that is red detuned by approximately a half linewidth from the $5s\,^2S_{1/2}$-$5p\,^2P_{1/2}$ line center [4,12,16]. In addition to cooling, the 422-nm laser performs state detection and state preparation.

The 422-nm beam enters through an optical access port of the vacuum chamber (vertical direction) that provides approximately equal projections for cooling along each of the three canonical directions of ion motion. A repumper laser at 1092 nm prevents the ion from decaying to the metastable $^2D_{3/2}$ state from the $^2P_{1/2}$ state. With these laser sources, the average ion kinetic temperature reaches ≈ 2 mK, slightly higher than the Doppler-cooling limit of 0.5 mK for $^{88}Sr^{+}$. A broadband and unpolarized repumping source was developed recently for the $^{88}Sr^{+}$ ion, yielding a lower ion temperature of 1.0 to 1.5 mK [17]. The broadband repumper was not used in the current experiments.

We have also determined the ion heating rates in our end-cap trap by measuring ion temperatures as a function of delay after the cooling pulses [18]. The temperatures were determined by comparing the relative strengths of the secular sidebands and carrier in the low-intensity limit [19,20]. We found a heating rate, averaged over the three canonical directions of motion,

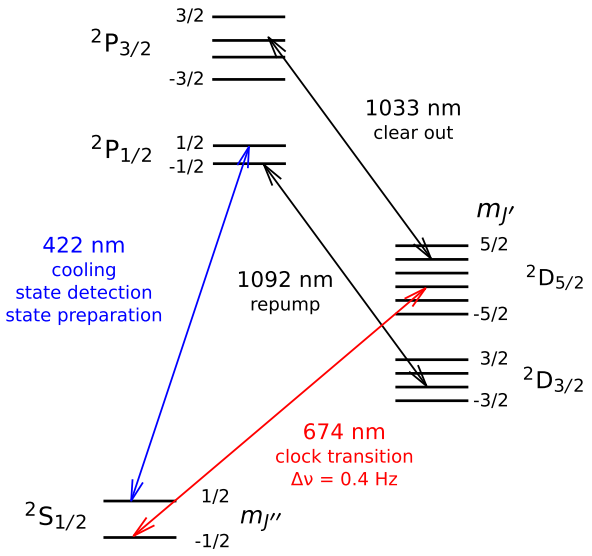

FIG. 1. (Color online) $^{88}Sr^+$ partial energy-level diagram. The solid lines show the laser wavelengths used to operate the optical frequency standard. The reference frequency is realized by the $5s\ ^2S_{1/2}$ - $4d\ ^2D_{5/2}$ electric-quadrupole transition at 674 nm (445 THz).

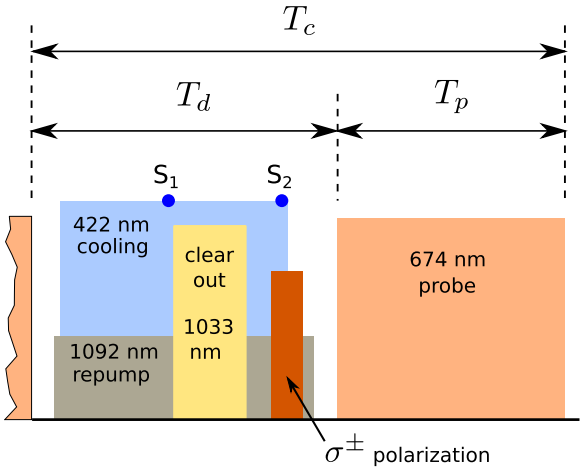

FIG. 2. (Color online) Pulse sequence for one interrogation cycle. In the experiments reported here, the dead time is $T_d = 28$ ms, and the probe pulse length varies from $T_p = 53$ ms to $T_p = 118$ ms. The time for one cycle is $T_c = T_d + T_p$. The durations of the 422-, 1092-, and 1033-nm laser pulses are, respectively, 22, 24, and 7 ms. The 422-nm polarization is switched from linear to circular ($\sigma^{\pm}$) for a duration of 4 ms and starts about 2 ms before the end of the pulse. The fluorescence level is sampled at S_1 for state detection and at S_2 to verify that the ion has returned to the ground state after the clear-out pulse.

of 3.5(8) mK/s. This corresponds to an increase in the average vibrational quantum number $\langle n \rangle$ of 61(14) quanta/s for radial motion and 32(7) quanta/s for axial motion.

A diode laser at 1033 nm is used to "clear out" the $^2D_{5/2}$ metastable state at each cycle, to return the ion to the ground state before the next interrogation pulse. Both the 1033- and 1092-nm lasers are frequency stabilized using a transfer Fabry-Pérot cavity referenced to a polarization-stabilized helium-neon laser [21]. Note that the use of broadband repumper and clear-out sources would circumvent the need for frequency stabilization [17].

The end-cap trap, described in detail elsewhere [12], was operated with a voltage amplitude of 212(4) V at a frequency of 14.408 MHz [22]. This particular choice of drive frequency reduces the micromotion shifts of the $^{88}Sr^+$ ion by a factor of at least 200 [7,22]. For these operating conditions, the radial and axial secular frequencies are, respectively, $f_r \simeq 1.2$ MHz and $f_z \simeq 2.3$ MHz.

The reader is referred to recent publications for a description of the end-cap trap, the uncertainty budget, and additional details about the laser systems [4,12,14].

B. Pulse sequence

Figure 2 shows the pulse sequence used in the present experiments. The total cycle time T_c is the sum of the pulse length and the dead time. The cooling and repump laser pulses occupy most of the dead time. There are 2-ms gaps at both ends of the probe pulses to ensure that all the other light sources are completely turned off during interrogation of the clock transition. The 1092-nm radiation remains on for about 2 ms longer than the 422-nm light to prevent unwanted decay to the $^2D_{3/2}$ metastable state during turn off of the cooling laser light.

During the cooling pulse, the ion state is first detected by monitoring the ion fluorescence at S_1. Shortly after, a clear-out pulse transfers the ion from the $^2D_{5/2}$ metastable state to the ground state via the short-lived $^2P_{3/2}$ state. This pulse is generated every cycle even if the ion is found in the ground state at S_1. The ion typically returns to the ground state in the early part of the clear-out pulse. The fluorescence level is monitored again at the end of the cooling pulse S_2 to verify that the clear out action was successful and that the ion was cooled for several milliseconds. This information is used to decide whether or not to include the next interrogation of the clock transition in the calculation of the transition probability used by the servo algorithm. The clear-out action is essentially 100% efficient. Cases when the ion is not detected in the ground state at S_2 are attributed to collisions with background gas.

The 422- and 1033-nm lasers are pulsed using mechanical shutters because they interact with transitions that share a common level with the clock transition. They require nearly perfect extinction to prevent light shifts. The 674- and 1092-nm lasers are modulated using acousto-optic modulators (AOMs).

The polarization of the 422-nm laser is briefly switched from linear to circular at the end of the cooling pulse for optical pumping of the ion into the ground-state magnetic sublevel of the probed transition. State preparation is further discussed in Sec. II C.

The dead time of 28 ms is determined by the 422-nm fluorescence collection efficiency of the optical system. The observed count rate of ≈ 5000 photons/s in our end-cap trap system gives, on average, 50 photons after 10 ms to determine the ion state.

C. State preparation

The $^{88}Sr^+$ ion has two ground-state magnetic sublevels with equal probabilities of being populated after interaction

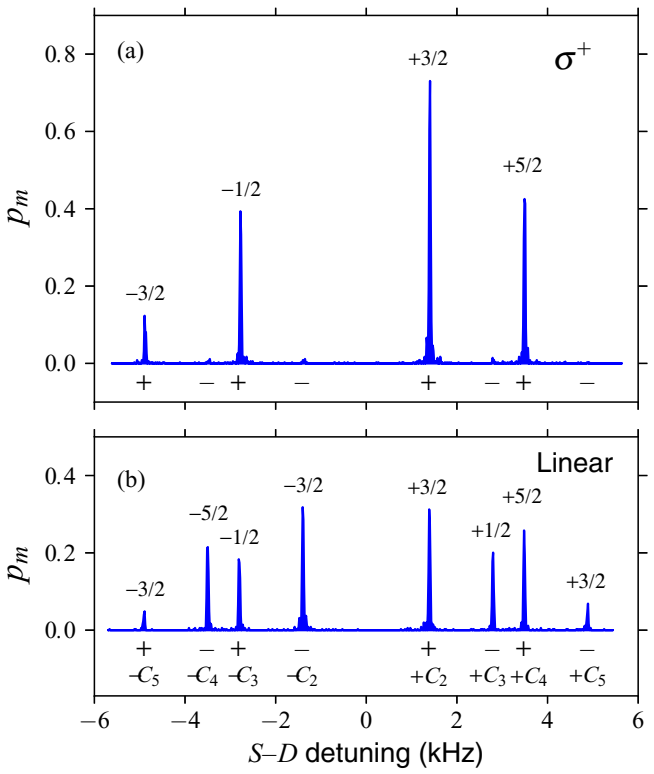

FIG. 3. (Color online) Zeeman-resolved spectra of the S-D transition of $^{88}Sr^{+}$ showing transition probability to the $^2D_{5/2}$ metastable state p_m as a function of laser detuning. The spectra were recorded with a magnetic field of 0.126 μT aligned along the 422-nm laser beam propagation direction for optical pumping using the S-P cooling transition. Zeeman components are labeled using $\pm C_x$, where x varies from 1 to 5 in order of increasing splitting. The C_1 pair is missing because the intensities of $\Delta m_J = 0$ transitions vanish when the probe laser propagation direction is perpendicular to that of the magnetic field [23]. The ground-state sublevel, $m_{J''} = \pm 1/2$, is shown below each Zeeman component by a + or a − sign, and the upper state sublevel, $m_{J'}(^2D_{5/2})$, is shown above the components. (a) Spectrum recorded with circularly polarized (σ^+) 422-nm light during the last 2 ms of the pulse. The ion is transferred to $m_{J''} = +1/2$ with $\approx$ 99% efficiency. (b) Spectrum recorded with the same experimental conditions as in (a), except that the 422-nm light was linearly polarized.

with a linearly polarized cooling pulse. This is illustrated by the Zeeman-resolved spectrum shown in Fig. 3(b), where the symmetric components of each Zeeman pair have similar intensities, indicating that the $m_{J''} = \pm 1/2$ populations are approximately equal. In this case, the probe pulses statistically interact with the ion only half the time, thus degrading the lock stability. Compared to the state-prepared case, the stability is degraded by a factor of slightly more than $\sqrt{2}$ as a consequence of the binomial statistics of the quantum jumps [24].

State preparation can be achieved in a number of ways, and the method chosen depends on the energy-level structure of the ion and the requirements of the experiment. For example, $^{199}Hg^{+}$ and $^{171}Yb^{+}$ are state prepared simply by turning the repumper laser off before the cooling laser [25,26]. For $^{88}Sr^{+}$ and several other ions, other methods are used such as frequency-resolved optical pumping on the clock transition [27] or optical pumping using circularly polarized light on the cooling transition [28]. A quantum logic method has also been applied to make a deterministic state preparation of the $^{27}Al^{+}$ ion [29].

The state-preparation method implemented in our current setup is optical pumping using circularly polarized 422-nm light. A longitudinal Pockels cell followed by a quarter-wave plate provides a voltage-controlled wave plate on the 422-nm beam path. The voltage applied determines whether the polarization at the ion is linear, σ^- or σ^+. When no voltage is applied, the polarization is linear, the normal mode for state detection and cooling. The magnetic field at the ion is aligned in the direction of the laser beam propagation using three pairs of Helmholtz coils installed on the vacuum chamber optical access ports [12].

State preparation starts 2 ms before the 422-nm beam is turned off and stops 2 ms after to ensure that only circularly polarized light interacts with the ion before the beginning of the probe pulse (see Fig. 2). Figure 3(a) shows the effect of using state preparation with σ^+ light on the S-D Zeeman spectrum. The ion is found in the $m_{J''} = +1/2$ sublevel 99% of the time. The probe power chosen for the scan gave a pulse area of $\approx 0.76\pi$ for the strongest component.

The clear-out and state-preparation steps allow for an optimized transition probability that typically reaches 0.95(3) of the theoretical maximum calculated for our $^{88}Sr^{+}$ ion when the trap secular frequencies and the ion kinetic temperature are taken into account in the model described in Sec. III A.

III. ION CLOCK STABILITY

A. Theory

The probe laser frequency is locked to a resonance by measuring the transition probability on each side of the resonance by stepping the laser frequency by $\pm\delta$ Hz about the expected line-center position. The imbalance in the probabilities is used to evaluate the offset frequency of the laser from line center. This offset is also the correction signal E in our locking servo algorithm, given by [30]

$$E = G\left(\frac{p_B - p_R}{p_B + p_R}\right), \tag{1}$$

where G is a gain parameter and where p_B or p_R is the probability that the ion is found in the metastable state after interaction with a probe pulse. The subscripts B and R indicate, respectively, that the laser is blue detuned or red detuned from line center. Therefore, $p_B = p_m(\nu_0 + \delta + \epsilon)$ and $p_R = p_m(\nu_0 - \delta + \epsilon)$, where p_m is the transition probability line shape, ν_0 is the transition line center in hertz units, and ϵ is the offset between the predicted and actual line centers. The correction signal is normalized by the sum of the probabilities. This feature preserves the size of the frequency corrections in the event that probabilities decrease over time.

The frequency corrections of Eq. (1) are subjected to fluctuations in population measurements called quantum projection noise [24]. This fundamental source of noise determines a lower limit for the lock instability. The population measurements follow a binomial distribution with a variance given by $\sigma^2_{p_x} = p_x(1 - p_x)$, where p_x refers to either p_B or

p_R. The variance of E is also the variance of the frequency fluctuations in the lock when other sources of noise are neglected. It can be calculated using Eq. (1) and $\sigma_{p_x}^2$. The resulting Allan deviation for an averaging time τ and for a single atom is given by [31,32]

$$\sigma_y(\tau) = \left\langle \frac{\Delta\nu_{\rm rms}}{\nu_0} \right\rangle_\tau = \frac{G}{\nu_0}\sqrt{\left(\frac{1-p_x}{p_x}\right)\frac{T_c}{\tau}}, \qquad (2)$$

where T_c is the cycle time defined earlier. Equation (2) is valid for the frequency corrections of Eq. (1). It makes no assumption regarding the line-shape function and is equally valid for Rabi and Ramsey interrogation line shapes. Although a second-order integrating servo algorithm [33] is implemented in our system to track variations in cavity drift rate, the value of G is set to obtain an "exact" correction at each step to reduce the residual servo-tracking errors to a minimum. For this reason, the choice of G in our experiments is not arbitrary. If we define k_p as the slope of the discriminant $p_B - p_R$ evaluated at line center ($\epsilon = 0$), then $G = -2p_x/k_p$. Equation (2) becomes

$$\sigma_y(\tau) = \frac{-2}{k_p\,\nu_0}\sqrt{p_x(1-p_x)\frac{T_c}{\tau}} = \frac{-2\,\sigma_{p_x}}{k_p\,\nu_0}\sqrt{\frac{T_c}{\tau}}, \qquad (3)$$

in agreement with the result given in [32].

The slope is evaluated numerically by solving the density matrix equations for a three-level system [16,32–34]. The model includes the lifetime of the $^2D_{5/2}$ state, decay to the two ground-state magnetic sublevels, and the effect of ion temperature on transition probability [34–36]. The effect of dead time is included in the parameter T_c (see Fig. 2). Decay from the metastable state can also occur between the end of the probe pulse and state detection at S_1. We define the parameter $t_{\rm detect}$ as a time threshold for detection. If the ion decays before a time $t_{\rm detect}$ after the probe pulse, the ion will be detected in the ground state. If it decays after that time, the ion will be detected in the metastable state. This parameter depends on the delay between the end of the probe pulse and S_1 and also on the detection thresholds used in the data-acquisition software. In our experiment, this effect decreases the calculated transition probabilities by a factor of $\exp(-t_{\rm detect}/\tau_{\rm ion}) = 0.975$.

B. Optimization of the lock parameters

Optimization of the lock parameters has been discussed in detail in previous works [32–34]. For Rabi interrogation, the pulse length, the probe power, and the stepping frequency δ can be adjusted for this purpose.

Optimization can be simplified when considering the following observations. Stability can be improved when δ is allowed to vary. The gain in stability, however, is marginal compared to the stability obtained by stepping the frequency by the usual half width at half maximum, δ = HWHM. Figure 4 shows the calculated optimum detunings $\delta_{\rm opt}$ normalized by $\delta_{\rm HWHM}$ as a function of pulse length. The graph also shows the corresponding optimum normalized Allan deviation. For T_p in the range between 20 ms and the optimum at 636 ms, the improvements in stability are below the 1% level.

The probe laser power would ideally be adjusted to optimize stability. Experimentally, it is more convenient to adjust the laser power to maximize the transition probability on resonance. This approach gives nearly optimal results, with a loss of stability of less than 1% for our typical operating parameters.

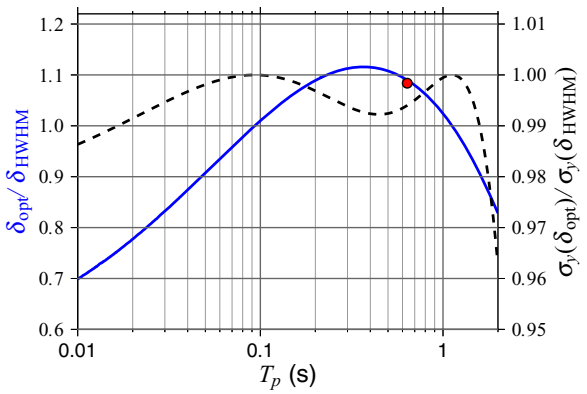

FIG. 4. (Color online) Minimization of the Allan deviation by varying the stepping frequency δ as a function of pulse length T_p. The solid line and left y axis give the optimum normalized stepping frequency $\delta_{\rm opt}/\delta_{\rm HWHM}$ as a function of T_p. The Allan deviation using $\delta_{\rm opt}$ normalized to the Allan deviation using $\delta_{\rm HWHM}$ is given by the dashed line and right y axis. The small circle shows the pulse length and stepping frequency that yield the overall best stability for Rabi interrogation [32]. The simulation was done for an ion in the lowest vibrational level, $\langle n\rangle = 0$, and for zero dead time.

When we prepare an experiment, we first decide on a pulse length T_p. The optimum gain is then calculated for δ = HWHM and for a pulse area that gives the maximum transition probability on resonance. This optimization procedure gives a theoretical stability level within $\approx 2\%$ of the fully optimized value for Rabi interrogation.

C. Lock method

The $^{88}Sr^+$ ion clock transition has no magnetic insensitive resonance, a consequence of its spinless nucleus. Instead, there are ten allowed Zeeman transitions, arranged as five symmetric pairs. The linear Zeeman effect is canceled by averaging the center frequencies of two components that have equal and opposite Zeeman shifts.

It was found that other important shifts could be canceled by averaging the frequencies of Zeeman pairs that connect to all of the $^2D_{5/2}$ state sublevels [12,15,37]. For this reason, we usually operate the lock by measuring the frequencies of six Zeeman components from three symmetric pairs that probe all the sublevels of the $^2D_{5/2}$ metastable state. The symmetric pairs used in the present work, C_2, C_3, and C_4, fulfill this requirement. The linear polarization of the probe laser was adjusted to obtain similar intensities on these components.

The lock algorithm operates by locking independently to the six Zeeman components. The lock cycles continuously through a predetermined sequence. The only information shared between the locks to individual components is the evaluation of the cavity drift rate made by the second-order integrating servo. When switching to the next component in the cycle, its predicted line-center frequency is calculated based

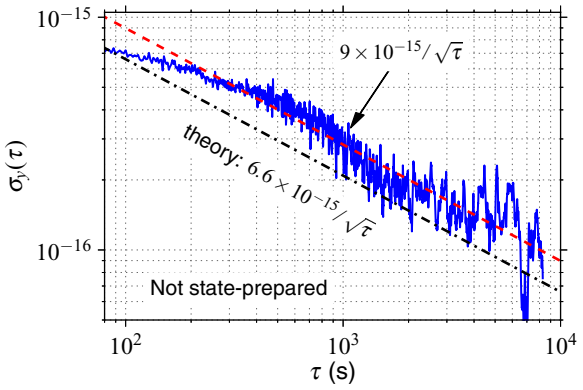

FIG. 5. (Color online) Single-clock Allan deviation as a function of averaging time obtained from a comparison between two $^{88}Sr^{+}$ ion clocks. The Allan deviation was divided by $\sqrt{2}$ to obtain the single-clock performance. The solid line is the data, and the dashed line is a $\tau^{-1/2}$ fit. The dot-dashed line is the calculated Allan deviation for the experimental conditions of the measurements. Neither system had state preparation implemented. Both locks were operated with $T_p = 53$ ms and $T_d = 28$ ms. Each Zeeman component was probed for a period 10 s (5 s per side) for a total of 60 s per cycle over the three pairs of Zeeman components.

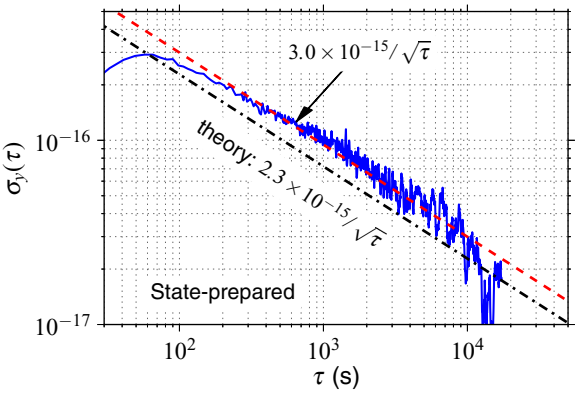

FIG. 6. (Color online) Single-clock Allan deviation of a state-prepared $^{88}Sr^{+}$ ion as a function of averaging time. The data shown as the solid line were obtained using self-comparison measurements. (See text for details.) The dashed line is a fit showing the stability achieved. The dot-dashed line is the calculated Allan deviation. The lock was operated with $T_p = 118$ ms and $T_d = 28$ ms. Each Zeeman component was probed for a period of 8 s (4 s per side) for a total of 48 s per cycle over the three pairs of Zeeman components.

on its previous value, the elapsed time since that value was measured, and the current cavity drift rate.

The six line centers are averaged in software to obtain a highly unbiased S-D line-center frequency. The data can also be used for diagnostics, for example, to obtain the line centers of each pair of components, the variations in magnetic field from the Zeeman splittings, etc.

For optimum lock stability, we find experimentally the laser intensities that maximize the transition probabilities of the three Zeeman pairs. The laser intensity is controlled with a double-pass AOM that creates the interrogation pulses and tunes the laser frequency [12].

D. Results

Figure 5 shows an Allan deviation as a function of averaging time obtained by comparing two $^{88}Sr^{+}$ ion optical frequency standards. One standard uses a trap based on the end-cap design with an evaluated uncertainty of 1.2×10^{-17} in fractional frequency units [7,12]. The other standard uses a Paul-type quadrupole ion trap, with an uncertainty estimated at $\approx 1 \times 10^{-16}$, caused mainly by imperfectly suppressed micromotion shifts [7]. The measurement reported in Fig. 5 was made with a clear-out step but without state preparation of the ground state. The observed stability of $9 \times 10^{-15}/\sqrt{\tau}$ is in reasonable agreement with the calculated stability of $6.6 \times 10^{-15}/\sqrt{\tau}$.

For stability measurements at the QPN limit, the Paul trap has some limitations compared to the end-cap trap. First, it has a single μ-metal shield to protect the ion from variations in the laboratory magnetic field [38]. The end-cap trap has two shields. As a consequence, the frequency noise caused by Zeeman splitting fluctuations, a known cause for stability degradation [39], is about an order of magnitude larger in the Paul trap than in the end-cap trap. In addition, the maximum transition probability obtained with the Paul trap is usually smaller than that of the end-cap trap, by about 25%.

For these reasons, we have performed stability measurements using self-comparisons in the end-cap trap. As described in Sec. III C, the probe laser frequency is locked to the C_2, C_3, and C_4 symmetric pairs. Allan deviations can be calculated for all possible combinations, C_2 vs C_3, C_2 vs C_4, and C_3 vs C_4. The average frequency offset between two symmetric pairs is removed before the Allan deviation is calculated because each pair has a different center frequency caused by the $m_{J'}^2$ dependence of the electric quadrupole shift. The three Allan deviations from each run are averaged, and the result is divided by $\sqrt{6}$ to obtain the single-clock stability. This correction factor includes the usual $\sqrt{2}$ instability increase caused by the comparison of two clocks and an additional $\sqrt{3}$ factor caused by the sequential measurement of three pairs of components that results in each pair being measured only one third of the time [12]. Figure 6 shows an Allan deviation for a pulse length of $T_p = 118$ ms. The observed stability of $3 \times 10^{-15}/\sqrt{\tau}$ is in good agreement with the calculated QPN limit of $2.3 \times 10^{-15}/\sqrt{\tau}$ that assumes negligible laser and Zeeman splitting frequency noise.

In light of the low uncertainty on the systematic shifts obtained in the end-cap trap, self-comparison measurements are actually expected to yield worse stability at long averaging times than comparisons between two traps with the same high-performance levels. The main reason is that the center frequency of each symmetric Zeeman pair is subject to changes in its electric quadrupole shift either through changes in the magnetic field direction or in the electric-field gradient at the ion. In contrast, when two traps are operated independently, these shifts are canceled to a very high level by averaging the center frequencies of several pairs. The stability of $\approx 2 \times 10^{-17}$ observed in Fig. 6 after 20 000 s of averaging suggests that the electric quadrupole shifts at the 10^{-14} level remained quite stable during this measurement run. This is a typical behavior for the measurements reported here.

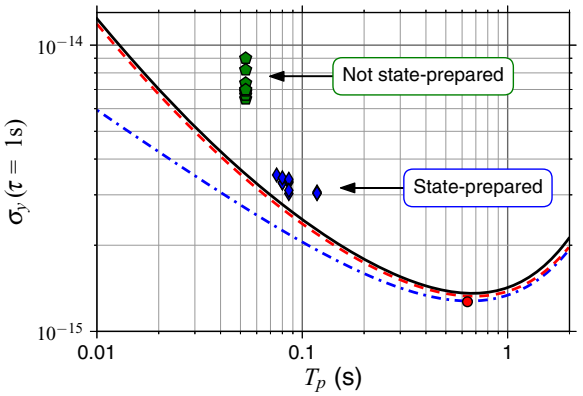

FIG. 7. (Color online) Summary of 1-s stability measurements made at various interrogation pulse lengths. The pentagons were made without state preparation of the ground state, and the diamonds were made with state preparation. A clear-out step was used in all cases. The dot-dashed line is the Allan deviation calculated for Rabi interrogation limited by only QPN. The dashed line includes the effect of a 28-ms dead time and a 10-ms detection time. The solid line includes in addition the effect of a 2 mK ion temperature. The optimum stability of $1.27 \times 10^{-15}/\sqrt{\tau}$ is found at $T_p = 0.636\text{s} = 1.628\ \tau_{\text{ion}}$, as shown by the small circle, in agreement with the optimized parameters reported in [32].

The common-mode shifts in the self-comparison, those that affect the different Zeeman pairs by the same amount, are all $\lesssim 1 \times 10^{-17}$ for the $^{88}Sr^+$ ion standard [4,7,12]. An instability at that level would not be observed in a trap comparison for the averaging times used in the current study. Another observation is that self-comparison measurements are asynchronous. They cannot benefit from laser noise reduction obtained in a synchronous frequency comparison of two optical standards [40].

Figure 7 summarizes the results from several stability measurements made at various pulse lengths. The data points obtained without state preparation include both two-trap and self-comparisons. The curves are Allan deviations evaluated using a density-matrix model of the line shapes and transition probabilities. They show that an ion temperature at the 2 mK level in a trap with an axial secular frequency of 2.3 MHz produces a very small degradation of stability. Dead time has a somewhat more noticeable effect.

The state-prepared data show stabilities reaching $3 \times 10^{-15}/\sqrt{\tau}$ for pulse lengths of $\gtrsim 86$ ms, in good agreement with the QPN limit when the effect of dead time is included. To our knowledge, this is one of the lowest instabilities reported for a single-ion standard [1,2].

As expected, the observed instabilities are slightly higher than the theoretical limit because laser frequency noise [41] and Zeeman splitting noise [39] were not included in the model. The lack of improvement observed beyond $T_p = 86$ ms in Fig. 7 may be an indication that laser frequency noise begins to degrade stability for longer pulse lengths.

The $^{88}Sr^+$ ion standard stability is ultimately limited by its upper state lifetime of 0.4 s. For Rabi interrogation this limit is $1.27 \times 10^{-15}/\sqrt{\tau}$ for a pulse length of $T_p = 0.636$ s. For Ramsey interrogation [42,43], this limit is $1 \times 10^{-15}/\sqrt{\tau}$ for an interrogation time of $\tau_{\text{ion}} \simeq 0.4$ s [32].

An interesting property of Ramsey interrogation is that its instability is ≈ 1.5 times lower than that obtained with Rabi pulses for the same interrogation time. This gain is valid over a wide range of interrogations times shorter than τ_{ion}. We assumed here that each Ramsey pulse has a duration of 10% the total interrogation time to mitigate issues such as light shifts and sensitivity to AOM chirps [44].

Further improvements in stability will necessitate better control of the probe laser frequency noise and of the magnetic field noise. The laser frequency noise in our system could be improved with a cavity design that further reduces thermal noise and vibration sensitivity [45–48]. Other sources of laser frequency noise to consider are the effect of residual amplitude modulation in the phase modulation used for locking to the ultrastable cavity [49], beam transport from a reference mirror on the optical table to the trapped ion [50], and phase chirps in the double-pass AOM used for controlling the probe laser frequency and timing [44]. The stability could also be improved by shortening the dead time.

IV. CONCLUSIONS

Stability is a crucial performance parameter of an optical clock that determines the averaging time required to reach a given level of statistical uncertainty in a frequency measurement. The recent control of the systematic shifts at the 10^{-17} to 10^{-18} level observed with optical clocks emphasizes the benefits of operating them near their optimum stability.

We have presented in this paper improvements made to our $^{88}Sr^+$ ion clock that yield a stability near the quantum projection noise limit for pulse lengths of $\lesssim 100$ ms. These improvements are the implementation of two optical pumping steps, one to clear out the metastable state after the ion state has been detected and another to prepare the ion in the ground-state magnetic sublevel of the probed transition. The ion prepared in this manner interacts with the probe pulse at every cycle. The stability obtained is $3 \times 10^{-15}/\sqrt{\tau}$, compared to $1 \times 10^{-14}/\sqrt{\tau}$ when these steps were not in place [12]. The benefits are substantial when considering the current evaluated uncertainty of 1.2×10^{-17} for our $^{88}Sr^+$ ion clock [7]. Prior to implementation of the optical pumping steps, it would have taken two weeks to reach this uncertainty level in a clock comparison, while it should now take 1.5 days. The stability obtained compares well with the best stability demonstrated for a single-ion standard of $2 \times 10^{-15}/\sqrt{\tau}$ [2].

As mentioned earlier, the 1.2×10^{-17} fractional frequency uncertainty of our $^{88}Sr^+$ ion clock is currently determined by the BBR field uncertainty. The projected performance with an improved measurement of the BBR field is $\lesssim 3 \times 10^{-18}$ [7]. It should be possible to further reduce the total uncertainty to $\approx 1 \times 10^{-18}$ using new trap and vacuum chamber designs aimed at reducing the BBR field uncertainty and the background gas pressure.

Avenues to improve the stability further were discussed, such as Ramsey pulse interrogation, reduction of frequency noise, and reduction of dead time. A stability of $1.5 \times 10^{-15}/\sqrt{\tau}$ is feasible for the $^{88}Sr^+$ single-ion system. It would allow comparison of two identical single-ion clocks with a statistical uncertainty of 3×10^{-18} in less than a week. The $1/\sqrt{\tau}$ averaging behavior assumed here requires good control

of the systematic shifts and of the experimental parameters for the duration of the measurements to avoid a degradation of the clock-comparison stability. For example, the probe laser powers delivered to the ions and the directions of the magnetic fields must remain constant at a level that maintains the quantum jump probabilities near their optimum values during the clock comparison.

ACKNOWLEDGMENTS

The authors would like to thank J. E. Bernard for the software implementation of the $^{88}Sr^{+}$ lock algorithm. The authors acknowledge the contributions of R. Pelletier, W. Pakulski, and B. Hoger in the design and fabrication of several electronic components used in the single-ion clock system.

[1] T. Rosenband, D. B. Hume, P. O. Schmidt, C. W. Chou, A. Brusch, L. Lorini, W. H. Oskay, R. E. Drullinger, T. M. Fortier, J. E. Stalnaker, S. A. Diddams, W. C. Swann, N. R. Newbury, W. M. Itano, D. J. Wineland, and J. C. Bergquist, Science **319**, 1808 (2008).

[2] C. W. Chou, D. B. Hume, J. C. J. Koelemeij, D. J. Wineland, and T. Rosenband, Phys. Rev. Lett. **104**, 070802 (2010).

[3] S. A. King, R. M. Godun, S. A. Webster, H. S. Margolis, L. A. M. Johnson, K. Szymaniec, P. E. G. Baird, and P. Gill, New J. Phys. **14**, 013045 (2012).

[4] A. A. Madej, P. Dubé, Z. Zhou, J. E. Bernard, and M. Gertsvolf, Phys. Rev. Lett. **109**, 203002 (2012).

[5] N. Huntemann, M. Okhapkin, B. Lipphardt, S. Weyers, Chr. Tamm, and E. Peik, Phys. Rev. Lett. **108**, 090801 (2012).

[6] N. Hinkley, J. A. Sherman, N. B. Phillips, M. Schioppo, N. D. Lemke, K. Beloy, M. Pizzocaro, C. W. Oates, and A. D. Ludlow, Science **341**, 1215 (2013).

[7] P. Dubé, A. A. Madej, M. Tibbo, and J. E. Bernard, Phys. Rev. Lett. **112**, 173002 (2014).

[8] G. P. Barwood, G. Huang, H. A. Klein, L. A. M. Johnson, S. A. King, H. S. Margolis, K. Szymaniec, and P. Gill, Phys. Rev. A **89**, 050501 (2014).

[9] B. J. Bloom, T. L. Nicholson, J. R. Williams, S. L. Campbell, M. Bishof, X. Zhang, W. Zhang, S. L. Bromley, and J. Ye, Nature (London) **506**, 71 (2014).

[10] I. Ushijima, M. Takamoto, M. Das, T. Ohkubo, and H. Katori, Nat. Photonics **9**, 185 (2015).

[11] T. L. Nicholson, S. L. Campbell, R. B. Hutson, G. E. Marti, B. J. Bloom, R. L. McNally, W. Zhang, M. D. Barrett, M. S. Safronova, G. F. Strouse, W. L. Tew, and J. Ye, Nat. Commun. **6**, 6896 (2015).

[12] P. Dubé, A. A. Madej, Z. Zhou, and J. E. Bernard, Phys. Rev. A **87**, 023806 (2013).

[13] V. Letchumanan, M. A. Wilson, P. Gill, and A. G. Sinclair, Phys. Rev. A **72**, 012509 (2005).

[14] P. Dubé, A. A. Madej, J. E. Bernard, L. Marmet, and A. D. Shiner, Appl. Phys. B **95**, 43 (2009).

[15] P. Dubé, A. A. Madej, J. E. Bernard, L. Marmet, J.-S. Boulanger, and S. Cundy, Phys. Rev. Lett. **95**, 033001 (2005).

[16] T. Lindvall, M. Merimaa, I. Tittonen, and A. A. Madej, Phys. Rev. A **86**, 033403 (2012).

[17] T. Fordell, T. Lindvall, P. Dubé, A. A. Madej, A. E. Wallin, and M. Merimaa, Opt. Lett. **40**, 1822 (2015).

[18] V. Letchumanan, G. Wilpers, M. Brownnutt, P. Gill, and A. G. Sinclair, Phys. Rev. A **75**, 063425 (2007).

[19] D. J. Berkeland, J. D. Miller, J. C. Bergquist, W. M. Itano, and D. J. Wineland, J. Appl. Phys. **83**, 5025 (1998).

[20] J. Keller, H. L. Partner, T. Burgermeister, and T. E. Mehlstäubler, J. Appl. Phys. **118**, 104501 (2015).

[21] G. Humphrey, Master's thesis, York University, 2009.

[22] P. Dubé, A. A. Madej, M. Tibbo, and J. E. Bernard, in *Proceedings of the 28th European Frequency and Time Forum* (IEEE, Neuchâtel, Switzerland, 2014), pp. 443–446.

[23] R. B. M. Clarke, Ph.D. thesis, University of Strathclyde, 1998.

[24] W. M. Itano, J. C. Bergquist, J. J. Bollinger, J. M. Gilligan, D. J. Heinzen, F. L. Moore, M. G. Raizen, and D. J. Wineland, Phys. Rev. A **47**, 3554 (1993).

[25] R. J. Rafac, B. C. Young, J. A. Beall, W. M. Itano, D. J. Wineland, and J. C. Bergquist, Phys. Rev. Lett. **85**, 2462 (2000).

[26] C. Tamm, D. Engelke, and V. Bühner, Phys. Rev. A **61**, 053405 (2000).

[27] C. F. Roos, M. Chwalla, K. Kim, M. Riebe, and R. Blatt, Nature (London) **443**, 316 (2006).

[28] G. P. Barwood, P. Gill, G. Huang, and H. A. Klein, Meas. Sci. Technol. **23**, 055201 (2012).

[29] P. O. Schmidt, T. Rosenband, C. Langer, W. M. Itano, J. C. Bergquist, and D. J. Wineland, Science **309**, 749 (2005).

[30] J. E. Bernard, L. Marmet, and A. A. Madej, Opt. Commun. **150**, 170 (1998).

[31] J. A. Barnes, A. R. Chi, L. S. Cutler, D. J. Healey, D. B. Leeson, T. E. McGunigal, J. A. Mullen, W. L. Smith, R. L. Sydnor, R. F. C. Vessot, and G. M. R. Winkler, IEEE Trans. Instrum. Meas. **20**, 105 (1971).

[32] E. Riis and A. G. Sinclair, J. Phys. B **37**, 4719 (2004).

[33] E. Peik, T. Schneider, and Chr. Tamm, J. Phys. B **39**, 145 (2006).

[34] C. Champenois, M. Houssin, C. Lisowski, M. Knoop, G. Hagel, M. Vedel, and F. Vedel, Phys. Lett. A **331**, 298 (2004).

[35] D. J. Wineland and W. M. Itano, Phys. Rev. A **20**, 1521 (1979).

[36] V. Letchumanan, P. Gill, E. Riis, and A. G. Sinclair, Phys. Rev. A **70**, 033419 (2004).

[37] P. Dubé, A. A. Madej, J. E. Bernard, and A. D. Shiner, in *Proceedings of the IEEE International Frequency Control Symposium and Exposition* (IEEE, New York, 2006), pp. 409–414.

[38] A. A. Madej, J. E. Bernard, P. Dubé, L. Marmet, and R. S. Windeler, Phys. Rev. A **70**, 012507 (2004).

[39] G. P. Barwood, G. Huang, S. A. King, H. A. Klein, and P. Gill, J. Phys. B **48**, 035401 (2015).

[40] M. Takamoto, T. Takano, and H. Katori, Nat. Photon. **5**, 288 (2011).

[41] A. D. Ludlow, T. Zelevinsky, G. K. Campbell, S. Blatt, M. M. Boyd, M. H. G. de Miranda, M. J. Martin, J. W. Thomsen, S. M. Foreman, J. Ye, T. M. Fortier, J. E. Stalnaker, S. A. Diddams, Y. L. Coq, Z. W. Barber, N. Poli, N. D. Lemke, K. M. Beck, and C. W. Oates, Science **319**, 1805 (2008).

[42] N. F. Ramsey, Phys. Rev. **78**, 695 (1950).

[43] J. C. Bergquist, S. A. Lee, and J. L. Hall, Phys. Rev. Lett. **38**, 159 (1977).

[44] C. Degenhardt, T. Nazarova, C. Lisdat, H. Stoehr, U. Sterr, and F. Riehle, IEEE Trans. Instrum. Meas. **54**, 771 (2005).

[45] J. Millo, D. V. Magalhães, C. Mandache, Y. Le Coq, E. M. L. English, P. G. Westergaard, J. Lodewyck, S. Bize, P. Lemonde, and G. Santarelli, Phys. Rev. A **79**, 053829 (2009).

[46] S. Webster and P. Gill, Opt. Lett. **36**, 3572 (2011).

[47] T. Kessler, C. Hagemann, C. Grebing, T. Legero, U. Sterr, F. Riehle, J. M. Martin, L. Chen, and J. Ye, Nat. Photonics **6**, 687 (2012).

[48] M. Bishof, X. Zhang, M. J. Martin, and J. Ye, Phys. Rev. Lett. **111**, 093604 (2013).

[49] W. Zhang, M. J. Martin, C. Benko, J. L. Hall, J. Ye, C. Hagemann, T. Legero, U. Sterr, F. Riehle, G. D. Cole, and M. Aspelmeyer, Opt. Lett. **39**, 1980 (2014).

[50] S. Falke, M. Misera, U. Sterr, and C. Lisdat, Appl. Phys. B **107**, 301 (2012).